DOING MORE WITH JUPITER'S MAGNETIC FIELD

J. E. P. Connerney*

Abstract

Jovian magnetic field models are based primarily on Pioneer 11 observations obtained in December 1974 and also to some extent on the Voyager 1 observations obtained in March, 1979. These spherical harmonic models have been very successful over the years in organizing a wealth of data, ranging from in–situ charged particle observations to remote observations of the aurora and radio emissions. In recent years the apparent lack of detailed agreement between model predictions and some observational inferences has become a subject of considerable interest. Examples include the position and intensity variation of the UV aurora, compared with the model Io flux tube footprint, and the frequency extent of decameter radio emissions as a function of Io's central meridional longitude, compared with computed surface field magnitudes. We are thus led to re–examine early estimates of Jovian field model uncertainties to determine reasonable limits on derived quantities of interest in modeling related phenomena (e.g., flux tube footprints). We also address the question of how to modify field models in a manner consistent with the in–situ magnetic field observations, and illustrate the effect of higher–order harmonics on the position of Io's flux tube footprint and the magnitude of the field along the footprint.

1 Introduction

The study of Jupiter's magnetosphere, initiated some 36 years ago by the discovery of radio emission from Jupiter [Burke and Franklin, 1955], has progressed remarkably in the last decade [see, e.g., quadrennial reports by Birmingham, 1983, Connerney, 1987, and McNutt, 1991]. In addition to radio wave observations gathered over the years [see, e.g. Carr et al., 1983], a wealth of in–situ and remote observations of Jupiter's magnetosphere became available with the Pioneer 10 and 11 spacecraft encounters in the early 1970's and the Voyager 1 and 2 spacecraft encounters of 1979. These encounters provided in–situ magnetic field and plasma observations, and maps of ultraviolet and infrared emissions associated with magnetospheric processes. Jupiter's relative proximity to Earth and the

*Laboratory for Extraterrestrial Physics, NASA Goddard Space Flight Center, Greenbelt, Maryland

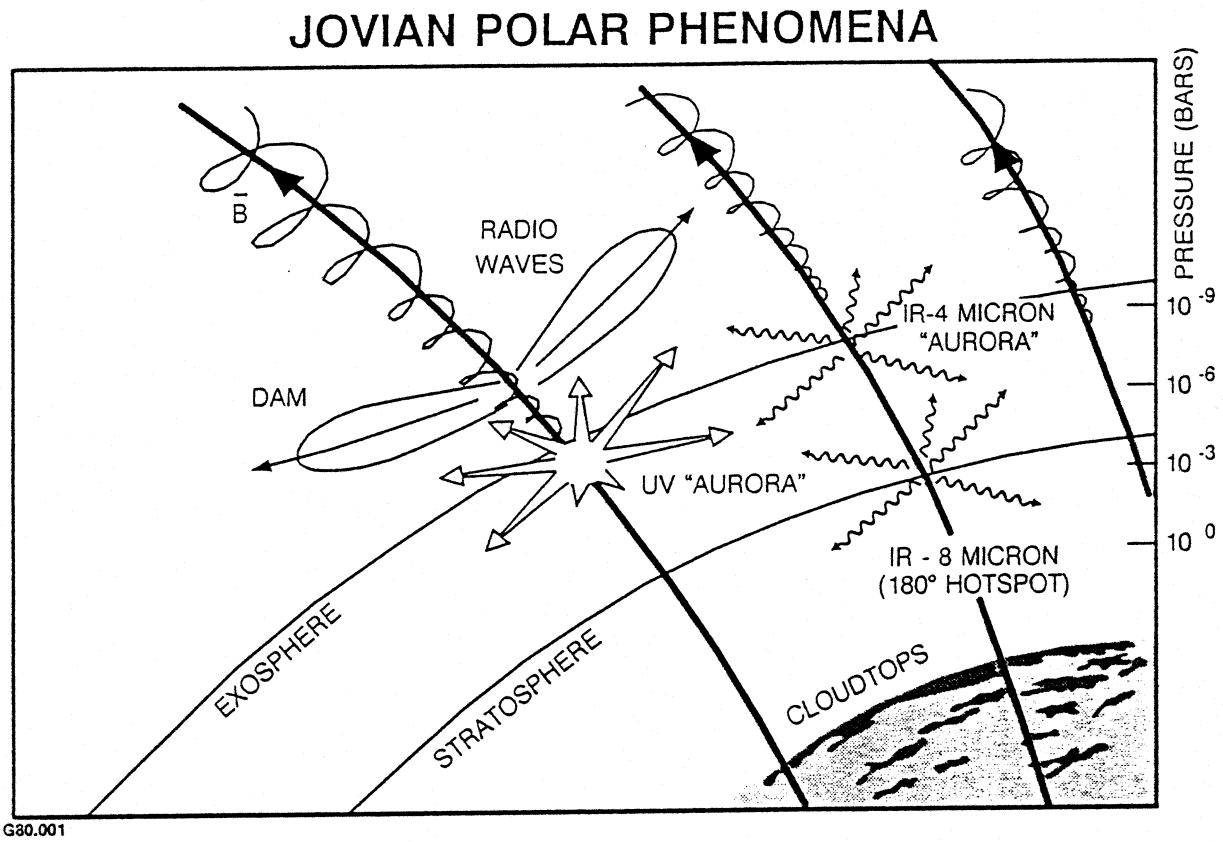

Figure 1: Schematic illustration of various emissions thought to originate in Jupiter's North polar region. Io–related decameter radiation, ultraviolet (UV) emissions from the vicinity of the Io foot, the localized thermal infrared (8 Micron) signature near 180°λ_{III}, and the 4 Micron distributed infrared emissions are shown.

sheer size of it's magnetosphere have made it a favorite target of observers confined to the Earth (and its immediate vicinity) as well. The 8–micron polar hotspot near the Io foot at 180°λ_{III} (Figure 1) has been studied extensively [e.g., Caldwell et al., 1983]. Synchrotron emission from the inner radiation belts has been mapped with impressive spatial resolution using the Very Large Array and modelled extensively [de Pater and Jaffe, 1984; de Pater, 1980]. Recent advances in technology now make possible images of Jupiter and the surrounding torus with ever–increasing temporal and spatial resolution. Examples include the optical images of the Io plasma torus by Schneider et al. [1991], and spatially–resolved infrared images of excited H_{3+} (aurorae?) in the Jovian polar region [Kim et al., 1991, and Baron et al., 1991]. Thus, models of these and other phenomena have been challenged both by observations of increasing resolution and diversity, and by the need to integrate in–situ and remote observations into a comprehensive model.

Considerable progress has been made in interpretation of these observations within the context of magnetic field models obtained from in–situ observations, most notably the octupole GSFC O_4 magnetic field model [Acuña and Ness, 1976a; 1976b] derived from Pioneer 11 observations. Such models are for the most part constrained to fit in–situ vector magnetometer observations along the spacecraft trajectory, subject to certain assumptions regarding the presence of local currents, for example, and the maximum order and degree

of the planetary field. The purpose of all such models is to predict the magnetic field in regions where it was not directly observed, that is, far from the spacecraft trajectory. The O_4 model has, in the 15 years since its introduction, been very successful in this regard. With it, Acuña and Ness [1976b] were able to identify the possible presence of a Jovian ring at 1.83 R_j radial distance. The presence of such a ring was subsequently confirmed by the optical detection of a ring at 1.81 R_j by the Voyager Imaging investigation [Smith et al., 1979]. Surface magnetic field magnitudes computed using the O_4 model reach a maximum of nearly 14 G in the northern hemisphere, by coincidence near the foot of Io's field line at λ_{III}=150° W longitude. This may be compared with the maximum frequency extent of Jovian DAM (39.5 and 38 MHz, Io–B and Io–A sources) if one assumes that emission occurs near the surface at the local electron gyrofrequency (f_c [MHz] =2.8 B [Gauss]). In contrast, the maximum field magnitude expected in the southern hemisphere is 10.4 G corresponding to a gyrofrequency of 29 MHz. This is sufficient for a non–Io D source (20 MHz), and nearly but not quite sufficient for both Io–C (30–32 MHz, but on occasion to 36 MHz) and non–Io C (<32 MHz). Many detailed comparisons of the morphology of Jovian radio emissions have been conducted, using modelled field directions and assumptions regarding the beaming of such emissions, with varying degrees of success [see review by Carr et al., 1983]. Likewise, detailed modelling of Jovian synchrotron radiation, originating near 1.5 R_j in the magnetic equator, has been performed [de Pater, 1980] using the O_4 model as well as the P11(3,2)A model of Davis et al., [1975].

While the field models have provided general agreement between observations and expectations, one often finds substantial differences if one looks closely enough. The inferred position of the UV aurora (Figure 2) deduced from Voyager Ultraviolet Spectrometer (UVS) observations is a good example. Recall that this Figure, from Broadfoot et al. [1981], represents but one of a number of exercises designed to locate the source of the UV auroral emissions. Since the projection of the UVS observing slit is rather large compared with the spatial scale of the aurorae, the source location must be done indirectly. This Figure is a result of the Voyager 2 post–encounter north–south map, in which the north–south oriented UVS slit repeatedly scanned from pole to pole. Both Voyagers remained very close to the Jovigraphic equator, so polar observations were necessarily made near the limb of the planet. The rotation of Jupiter brought different longitudes into the field of view as the slit scanned from pole to pole. Each closed circle in Figure 2 represents the maximum poleward extent of the UVS slit at a time when auroral emission was detected; correspondingly, each open circle represents the position of the poleward extent of the slit at times when auroral emission was not detected. Note that there are considerable challenges in accurately locating an observation made near the limb on a polar projection of this sort, since small pointing inaccuracies translate into considerable errors in the latitude of the poleward end of the slit. These errors remain to be quantified. Furthermore, one should not assume that these circles represent independent observations, given the method by which they were obtained and the expected sources of error. Nevertheless, the near–agreement of the UV–inferred auroral oval with the foot of the Io field line was initially considered remarkable; now we are troubled by the lack of agreement. While it appears that the UV aurora is associated with the Io foot, systematic differences can be seen, particularly near the southward extent of the oval at λ_{III} = 160° and opposite (λ_{III}=330°).

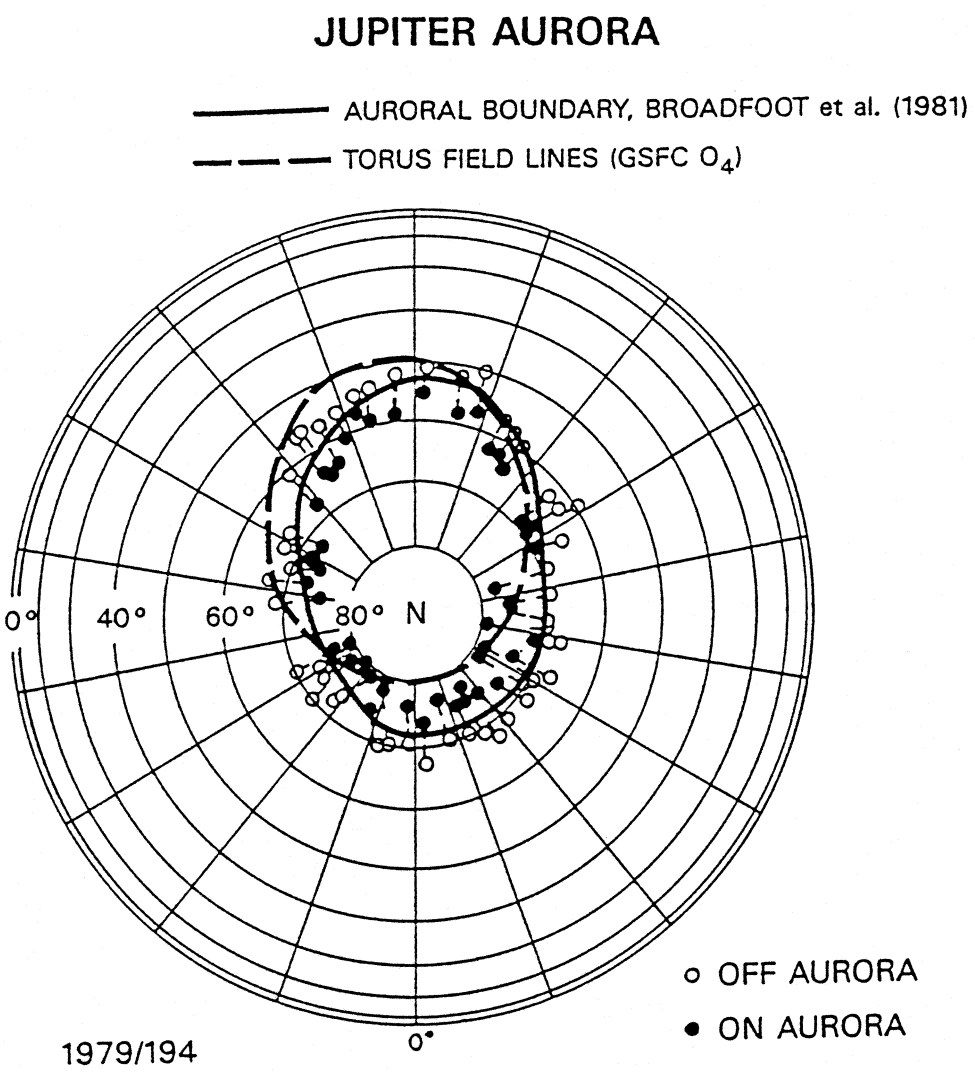

Figure 2: Map of UV observations of Jupiter's North pole deduced from Voyager Ultraviolet Spectrometer observations [Figure from Broadfoot et al, 1981], and the model Io footprint computed using the GSFC O_4 magnetic field model (dashed line). The location of auroral UV emissions was deduced by noting the position of the poleward end of the UVS slit, projected on the surface, at times when auroral emissions were detected (closed circles) and not detected (open circles). This is a polar projection of observations obtained during Voyager 2's relatively low–latitude departure from the Jovian system. Since the aurorae are observed near the limb of the planet, the projection of the position of the slit onto the pole is subject to pointing uncertainties which may be significant.

As a second example, we turn to statistical studies of the peak frequency of DAM as a function of Io's system III longitude [Genova and Aubier, 1987; Genova and Calvert, 1988; and Aubier et al., 1988]. These authors compared the high frequency limit of Io–dependent decameter radiation with the gyrofrequency at the foot of the Io field line (computed using the O_4 magnetic field model). While the peak observed frequencies were consistent with those attainable along the foot of Io's field line, it appeared that a

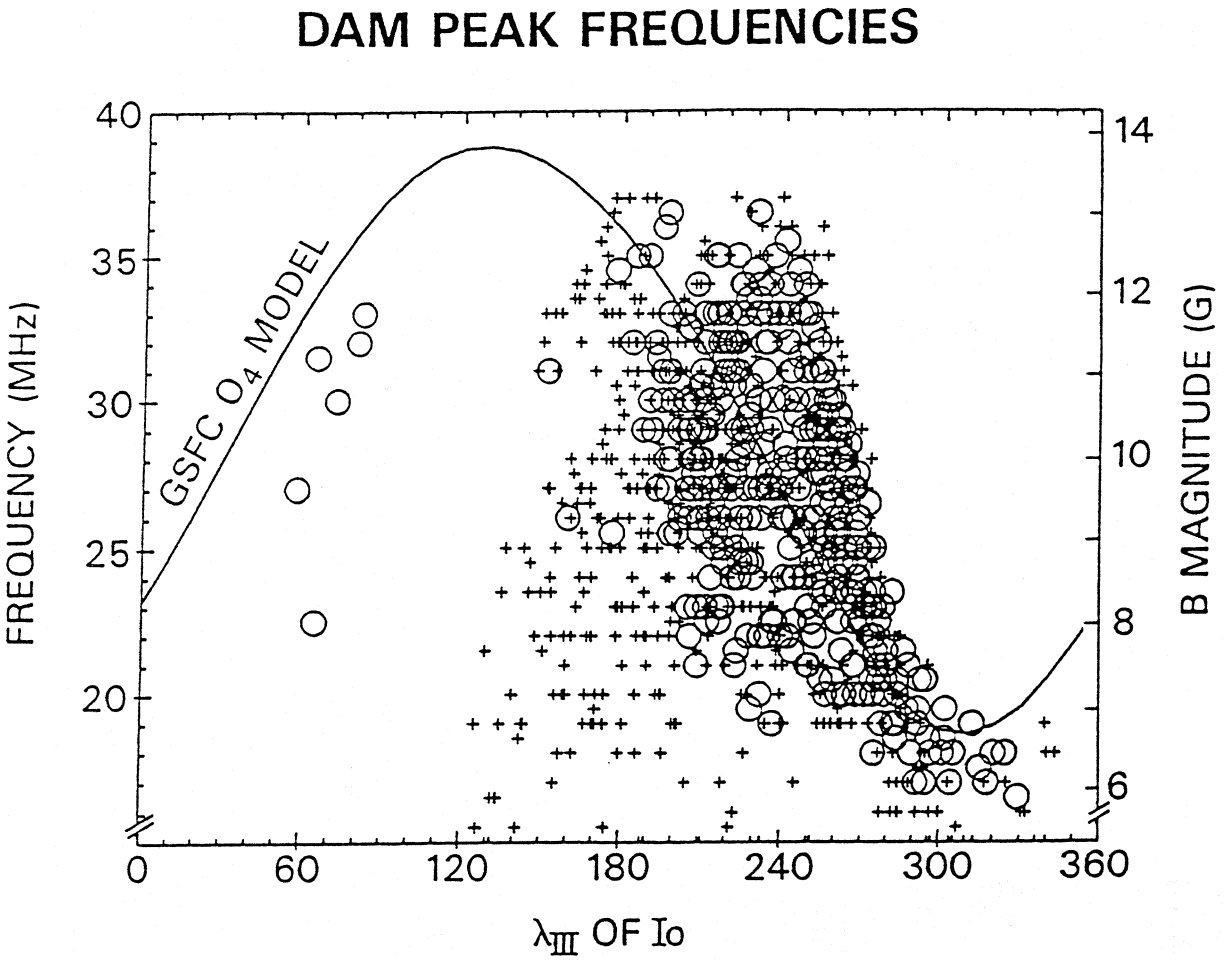

Figure 3: Frequency of Io–related decameter radiation as a function of Io's central meridian longitude (λ_{III}), compared with the magnetic field magnitude at the foot of the Io flux tube computed with the GSFC O_4 magnetic field model [Figure from Genova and Calvert, 1988].

70° shift in the computed field magnitudes as a function of λ_{III} was needed to reconcile the bulk of the observations and the model. Figure 3, from Genova and Calvert [1988], illustrates the apparent descrepancy. If one assumes that the peak frequency observed may be identified with the gyrofrequency at the foot of Io's field line, then the computed and inferred surface fields do not agree. However, as Aubier et al., [1988] point out, the 70° shift seemingly required to reconcile the peak frequencies would destroy the near–perfect agreement obtained with the GSFC O_4 model and several other independent studies of DAM.

In these and similar efforts, the question then arises: Is the lack of detailed agreement indicative of systematic errors in the observations, the theory, or the magnetic field model? The purpose of this paper is to examine the latter possibility, and to establish reasonable bounds on computed quantities of interest in modeling a variety of magnetospheric phenomena.

2 Jovian magnetic field models

Magnetic field models obtained from spacecraft flybys are necessarily non–unique, due to the spatial limitations on the available data. This fact has been well illustrated (perhaps too well) by Connerney's [1981] 'invisible planet', a hypothetical planet endowed with a magnetic field that is sizeable throughout most of space, but undetectable along the Pioneer 11 trajectory. Since the field models in general use today are based upon the Pioneer 11 observations, they are all subject to essentially the same non–uniqueness (not identically the same, since measurement errors may differ among different instruments). Using the singular value decomposition of the linear system, Connerney [1981] characterized the uncertainty of the GSFC O_4 model parameters, subject to the same assumptions made by Acuña and Ness [1976a]. Random noise on the measurements, and the spatial limitation of the observations, result in uncertainties of about $\pm$ 1 G (at 1 σ) in the computed surface field magnitudes. In this work, we would like to expand upon the earlier estimates of model parameter uncertainties by including the effects of heretofore unmodeled higher–order contributions to the field. In order to do this, we must first obtain a new model for the field, and a characterization of the model non–uniqueness.

The observed magnetospheric magnetic field can be regarded as the sum of contributions from several sources. Near the planet, the field is dominated by that due to the planetary dynamo (interior source); at greater distances, the magnetosphere becomes a magnetodisc, the field configuration distorted by an extensive washer–shaped ring current [Connerney et al., 1981]. The interaction of the planetary field with the solar wind leads to an insignificant field in the case of Jovian field models, and may safely be ignored. However, the magnetodisc contribution is significant, and must be accomodated in modelling efforts. In the case of the Pioneer 11 encounter observations, this source may be accomodated with either an explicit model of the magnetodisc or with an external spherical harmonic expansion. Either suffices, since the spacecraft did not appreciably penetrate the current–carrying region. The traditional spherical harmonic expansion of V is given by [e.g., Chapman and Bartels, 1940; Langel, 1987]

$$V = a \sum_{n=1}^{\infty} \left\{ \left(\frac{r}{a}\right)^n T_n^e + \left(\frac{a}{r}\right)^{n+1} T_n^i \right\} \tag{2.1}$$

where a is the equatorial radius of Jupiter (71 372 km). The first series in increasing powers of r represents contributions due to external sources, with

$$T_n^e = \sum_{m=0}^{n} \{P_n^m(\cos\theta)[G_n^m \cos(m\phi) + H_n^m \sin(m\phi)]\} . \tag{2.2}$$

The second series in inverse powers of r represents contributions due to the planetary field or internal sources, with

$$T_n^i = \sum_{m=0}^{n} \{P_n^m(\cos\theta)[g_n^m \cos(m\phi) + h_n^m \sin(m\phi)]\} . \tag{2.3}$$

The $P_n^m(\cos\theta)$ are Schmidt–normalized associated Legendre functions of degree n and order m, and the g_n^m, h_n^m and G_n^m, H_n^m are the internal and external Schmidt coefficients,

respectively. The angles θ and ϕ are the polar angles of a spherical coordinate system, θ (colatitude) measured from the axis of rotation and ϕ increasing in the direction of rotation. In cases where local currents must be explicitly modeled (e.g., Voyager 1 observations), the spherical harmonic expansion given above is augmented with a perturbation field, b, due to local currents. Both empirical [Connerney et al., 1982] and fully self–consistent magnetohydrodynamic models [Caudal and Connerney, 1989] have been utilized to calculate b; in this work, we use the former of the two to represent the field of the Jovian magnetodisc.

The traditional application of spherical harmonic analysis utilizes the orthogonality of the Legendre functions over the unit sphere. If the available observations are suitably distributed on the surface of a sphere, the Schmidt coefficients can be estimated independently. In usual practice, the series above is truncated at some maximum degree and order N_{max}, where N_{max} is sufficiently large to represent well the observed field, but not so large as to introduce more free parameters than can be determined from the observations. (The number of free parameters grows rapidly with increasing N_{max}, as $n_p = (N_{max} + 1)^2 - 1$. To the extent that the observations are globally distributed, estimates of the Schmidt coefficients are unaffected by the choice of N_{max}. If, on the other hand, the observations are poorly distributed or sparse, it will not be possible to uniquely determine all of the model parameters necessary to describe the planetary field. The Legendre functions are not orthogonal on the trajectory of the spacecraft, so in general estimates of the Schmidt coefficients cannot be independently determined. If an arbitrarily small choice of N_{max} is imposed upon the model, large errors in low–order terms will result from the neglect of higher–order terms with which they covary.

The Jovian field models in general use today were obtained under the assumption that the field is completely characterized by degree and order 1, 2, 3 (up to and including octupole); that higher–order moments are identically zero. This assumption is certainly not unreasonable, and with it one may find a complete solution to the linear system $y = Ax$ relating the observations (y) to the model parameters (x), the Schmidt coefficients of the spherical harmonic expansion. However, if appreciable higher–order contributions to the field exist, there are two problems to consider in attempting to quantify the uncertainties associated with certain model computations, e.g., the magnitude of the field at the foot of Io's field line, or the expected position of the aurora. The first is the most obvious: An estimate of the magnetic field computed with dipole, quadrupole, and octupole coefficients may differ from the true field by any amount, limited only by the magnitude of higher–order terms. Near the surface, contributions to the field from higher–order terms may be appreciable. The second problem associated with the presence of higher–order terms is less obvious but potentially more serious: Unmodeled higher–order contributions to the field measured by Pioneer 11 may be expected to influence estimates of the low–order terms, by virtue of the covariability of the Schmidt coefficients. In order to examine this question, we need repeat the analyses of Pioneer 11 observations, relaxing the assumption regarding the maximum degree and order spherical harmonic present. However, complete solutions to the linear system will no longer be possible, given the number of free parameters and the limited distribution of data. In order to constrain the parameters of the field to the maximum extent possible, we include Voyager 1 observations obtained in 1979 with the Pioneer 11 observations obtained in 1974; we assume the magnetic field has not changed

in that time, as indicated by independent analyses of both sets of data [Connerney and Acuña, 1982].

Each vector observation was weighted with the expected standard deviation of the observation, as is appropriate when observations from different statistical populations are utilized. This practice insures that each residual (the difference between an observation and a model field) is compared with its expected error. For the Pioneer 11 high field fluxgate observations, we use equal weights of 500 nT for each vector observation, consistent with the relatively large quantization stepsize of that instrument. Each of the Voyager 1 observations was weighted with equal weights of 10 nT; this figure is consistent with the accuracy of the magnetometer in the maximum field measured (∼3330 nT) and the attitude uncertainty of the Voyager spacecraft (∼0.1 degree, excepting certain spacecraft maneuvers). Pioneer 11 observations within the 5 R_j radial distance and Voyager observations within 10 R_j radial distance of the planet were used.

Construction of a partial solution via the singular value decomposition method silmultaneously minimizes the residual (difference between observed and modeled field) as well as the magnitude of the parameter vector needed to minimize the residual. A priori information regarding the magnetic field may be expressed in the form of parameter weighting. Previous analyses have demonstrated that the harmonic spectrum of the Jovimagnetic field (see next section) decreases with increasing degree and order, that is, the magnitude of the field due to higher–order moments decreases appreciably with increasing degree and order. We incorporate this knowledge into the inversion by weighting each parameter (Schmidt coefficient) with the weight $\left(\frac{r_c}{a}\right)^{n+2}$ where n is the degree of the corresponding Schmidt coefficient, a is Jupiter's radius, and r_c represents the presumed radius of the dynamo region, which we take as 0.7 R_j. This weighting results in a partial solution that favors adjustments to the low degree and order Schmidt coefficients (to achieve a given reduction in the model residuals) over those to high degree and order coefficients. This simply reflects our expectation that, on average, higher–order moments are likely to be of lesser magnitude than low–order moments.

The construction of partial solutions in fitting these observations is illustrated in Figure 4, which shows the weighted root–mean–squared (rms) residual (modeled − observed field) as a function of the number of eigenparameters included in the solution. This Figure illustrates the progressive improvement in modeling the data that results as more parameter vectors are included in the solution, for n less than or equal to about 18 or 22. Also shown in the Figure (filled points) are complete solutions to dipole, quadrupole, and octupole expansions; for example, the point labeled I2 represents a fit to a spherical harmonic model including terms to $N_{max} = 2$ in the internal field (dipole and quadrupole terms only, I2); likewise, the point labeled I3 represents a fit to a model including terms to $N_{max} = 3$ in the internal field (dipole, quadrupole, and octupole terms). The total number of free parameters available in any model is the sum of the $(N_{max} + 1)^2 - 1$ internal field parameters; there are 3 parameters available for a dipole model, 8 for a quadrupole, 15 for an octupole. A sixth order expansion offers a total of 48 parameters, most of which are not appreciably constrained by the available observations. The weighted rms of the data alone, with no model removed (1.0 in dimensionless units) is indicated in the Figure ('no model') as is the weighted rms expected of a model ('ideal') that fits the observations

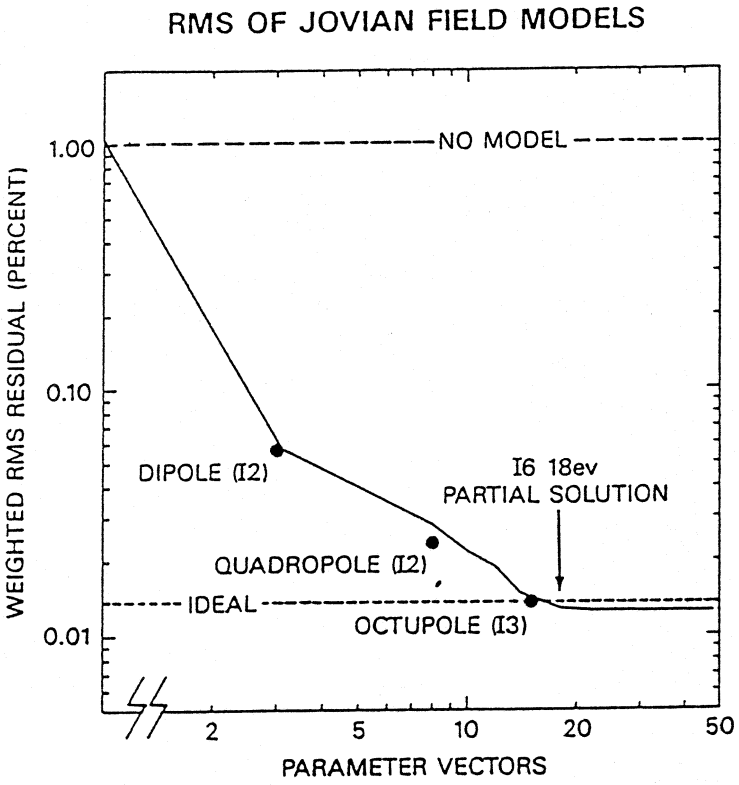

Figure 4: Weighted root–mean–squared (rms) residual (dimensionless) for partial solutions to a sixth–order spherical harmonic expansion (I6) of Jupiter's magnetic field as a function of the number of independent parameter vectors included in the partial solution. RMS residuals for complete linear solutions to a dipole (I1), quadrupole (I2), and octupole (I3) expansion are shown for comparison (filled circles).

within the standard error of observation (0.013 in dimensionless units). While neither a dipole or quadrupole model is capable of fitting the observations within observational error, an octupole is sufficient. The partial solution to the six–order expansion indicated in Figure 4 utilizes 18 parameter vectors, of a total 48 available, to achieve a weighted rms residual of 0.013 in dimensionless units. This model is referred to as the '18ev' model to emphasize that it represents a partial solution to the 6^{th} order spherical harmonic expansion, utilizing only 18 of the 48 eigenvectors, or orthogonal parameter vectors, of the linear system.

The low–order terms of the 18ev solution are listed in Table 1. As is the case with any partial solution, interpretation of the numerical results requires a careful consideration of the 'resolution matrix', R, which describes how well the partial solution approaches a complete solution, parameter by parameter. Our estimates of the Schmidt coefficients, based upon the κ–vector partial solution, x_κ, are related to the actual Schmidt coefficients we seek via the resolution matrix [Connerney, 1981]

$$x_\kappa = R \cdot x \tag{2.4}$$

where x_κ and x are both column vectors of length 48 (for the I6 expansion) and R is an 48 by 48 element square symmetric matrix. The i^{th} element of the estimated solution (parameter i) is the convolution of the i^{th} row of the resolution matrix with the solution of the complete linear system. In the case of a classical least–squares inversion, in which all parameter vectors are included in the solution, the resolution matrix is a unit diagonal matrix; there is a one–to–one correspondence between parameter estimates and

Table 1: Jupiter O_6 (18ev partial solution) and O_4 field models, Schmidt–normalized spherical harmonic coefficients. [Coefficients in Gauss, referenced to Jupiter system III (1965) coordinates, and 1 R_j= 71 372 km; O_6 model coefficients are given to 5 decimal places not as an indication of parameter accuracy but as an aid in converting Gauss to nanoteslas (ignore the decimal point). O_4 model coefficients as tabulated for system III (1965) by Acuña et al. [1983]; originally (1957 system III) from Acuña and Ness, [1976a].]

n	m	g(n,m)	(O_4)	h(n,m)	(O_4)
1	0	4.24202	(4.218)		
1	1	-0.65929	(-0.664)	0.24116	(0.264)
2	0	-0.02181	(-0.203)		
2	1	-0.71106	(-0.735)	-0.40304	(-0.469)
2	2	0.48714	(0.513)	0.07179	(0.088)
3	0	0.07565	(-0.233)		
3	1	-0.15493	(-0.076)	-0.38824	(-0.580)
3	2	0.19775	(0.168)	0.34243	(0.487)
3	3	-0.17958	(-0.231)	-0.22439	(-0.294)

actual parameters. As fewer parameter vectors are admitted in the solution, some of the off–diagonal elements grow at the expense of the diagonal elements, reflecting a loss of parameter resolution. Only those Schmidt coefficients listed in Table 1 are reasonably well resolved (resolution matrix diagonal >0.8). The remaining coefficients, of degree and order 4 and greater, are not significantly constrained by the available data and are not listed here.

We are thus led to adopt for present purposes a model field consisting of orders 1, 2 and 3 (dipole, quadrupole, and octupole) from Table 1, designated 'O_6', referring to the octupole (O) part of an sixth–order spherical harmonic model (partial solution). This model will form the basis of all Jovian models considered herein; additional models which are also consistent with the in–situ magnetometer observations, will be constructed by (pseudo–random) addition of linear combinations of the remaining (undetermined) parameter vectors.

3 Discussion of 'O_6' Jovian field model

The Jovian field model (18 ev) obtained as a partial solution to the sixth order expansion has a more Earth–like spectrum of higher–order moments than previous models (Figure 5). We compare the harmonic spectra with reference to

$$R_n = (n+1) \sum_{m=0}^{n} \left\{ (g_n^m)^2 + (h_n^m)^2 \right\} . \tag{3.1}$$

This quantity, used in studies of the geomagnetic field [Lowes, 1974; Langel and Estes, 1982], is equal to the mean squared magnetic field intensity over the planet's surface

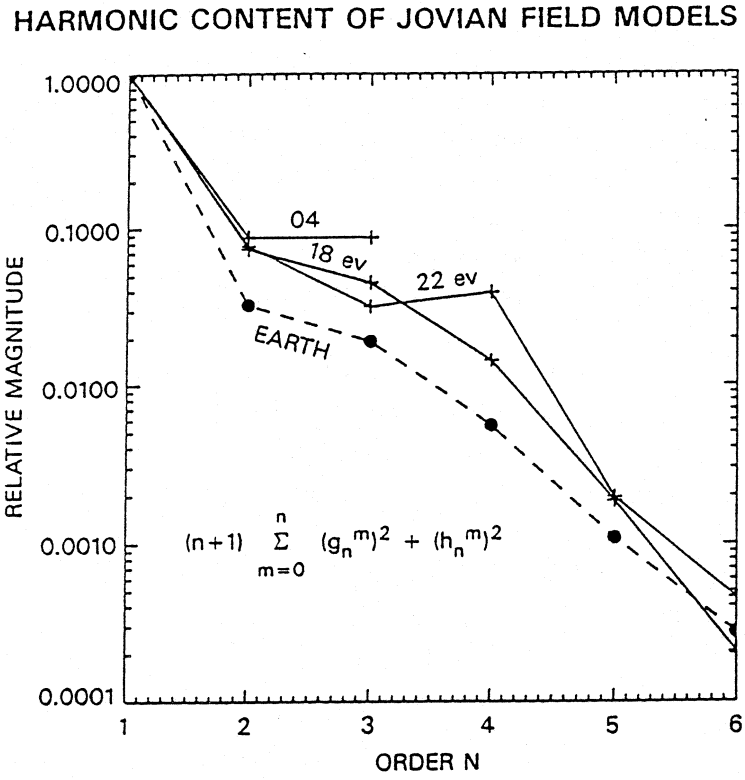

Figure 5: Normalized harmonic content of Jovian magnetic field models, compared with that of the Earth, up to order and degree n=6. The 18 and 22 eigenvector partial solutions illustrated here are characterized by relatively low higher–order harmonics (n>3) but none of these coefficients are constrained by the Pioneer 11 and Voyager 1 magnetic field observations. Both models are considerably more 'Earth–like' than the O_4 model in the relative magnitude of the octupole moment.

produced by harmonics of degree n. In Figure 5 we show R_n as a function of n for two Jovian field models that represent partial solutions to an I6 internal field (inclusion of 18 and 22 parameter vectors), the O_4 model of Acuña and Ness [1976a], and the GSFC 12/83 model [Langel and Estes, 1982] of the Earth's magnetic field. Scaled to the core–mantle boundary with the factor $\left(\frac{a}{r_c}\right)^{2n+4}$, the terrestrial spectrum becomes almost flat for $n \leq 14$, suggesting a 'white' spectrum for the dynamo at the core–mantle boundary [e.g., Lowes, 1974; Langel and Estes, 1982]. It is assumed that the core–mantle boundary, the location of which is very accurately known, represents the outer boundary of the geodynamo.

These partial solutions evidence smaller higher–order moments for several reasons. The parameter weighting employed herein actively discourages large higher–order moments in accordance with the a priori assumption that the Jovian dynamo produces a 'white' spectrum at a core radius $< 1\ R_j$, reflected in the parameter weighting. Having relaxed the assumption that all terms with n>3 are identically zero, it is now possible to represent the observed field with lesser quadrupole and octupole moments. Finally, with the use of both Pioneer 11 and Voyager 1 observations, parameter standard deviations are considerably reduced, leading to reduced quadrupole and octupole moments by virtue of the positive definite nature of the computed moments. (The appearence of 'noise' in a Figure such as Figure 5 will result in a less steep spectrum with increasing degree.)

The O_6 model parameters compare favorably with those of the O_4 model of Acuña and Ness [1976a] and the V1 17ev model [Connerney et al., 1982] with a few notable exceptions, predominantly among the octupole terms. A few terms differ by more than 2 standard deviations [Connerney, 1981]; in general, the difference is such that the larger octupole coefficients of the O_4 model are considerably reduced (as is the quadrupole g_2^0 term). The

net effect is to produce a field that is more 'Earth–like' than O_4. Figure 6 compares the inferred position of the Io footprint calculated for the O_4 and O_6 field models. The UV aurora observations and the footprint of 'open' field lines are shown as well. Clearly, the new Io footprint still differs appreciably from the locus of inferred UV aurora positions. Field magnitudes (and gyrofrequencies) along the Io footprint, computed using both O_4 (dashed) and O_6 (solid line) may be compared with reference to Figures 7 and 8. In Figure 7, the field magnitudes are plotted as a function of the longitude (λ_{III}) of the Io footprint *at the surface*; in Figure 8, the field magnitude is plotted as a function of Io's longitude (λ_{III}) at r=5.95 R_j radial distance in the Jovigraphic equator. The two presentations differ appreciably due to the 'twist' of field lines traced from Io to the surface. Field lines which are equidistant along Io's orbit are 'bunched' towards the regions of higher field magnitude at the surface (not a phase shift in any one direction). The peak field magnitude in both polar regions along the Io footprint is only slightly greater for the O_6 model, compared with the O_4 model. The magnitude of the variation in longitude is considerably less for the O_6 model in both polar regions (i.e., the model is more 'Earth–like').

4 Putative Jovian field models

The parameter vectors which have been excluded from the partial solution obtained here are poorly constrained by the available magnetic field observations. One may therefore add or subtract a suitable linear combination of these excluded parameter vectors to any proposed Jovian field model without significantly degrading the fit to the available observations. This suggests a convenient procedure for constructing *possible* alternative field models which are also consistent with the available magnetic field observations. We simply form a model perturbation as a weighted linear sum of all of the orthonormal parameter vectors, allowing for a 1 or 2σ variation on the data [see appendix in Connerney et al., 1991 for details], weighting each parameter vector with a weight assigned by a Gaussian random number generator. All models generated in this fashion are acceptable alternatives to the models listed in Table 1, or for that matter *any* model derived from the Pioneer 11 and Voyager 1 observations.

The combined Pioneer 11 and Voyager 1 observations are not sufficient to constrain the magnitude of higher degree and order terms ($n > 3$). Alternative models constructed as described above exhibit unreasonably large higher–order moments. This is, of course, an expected consequence of the propagation of 'noise' into the higher–order coefficients.

Figure 6: (next page, color plot) Orthographic polar projection of the magnitude of the magnetic field on the surface of Jupiter computed using the O_6 model. Colors are assigned to field magnitudes in accordance with the color scale to the right of the Figure. Also shown is the foot of the Io field line computed using the O_6 model (solid line), the GSFC O_4 model (dashed), and the inferred positions of the UVS aurora (closed and open circles) as in Figure 2 [from Broadfoot et al., 1981]. The inner solid line approximately traces the foot of the last closed field line using the O_6 model.

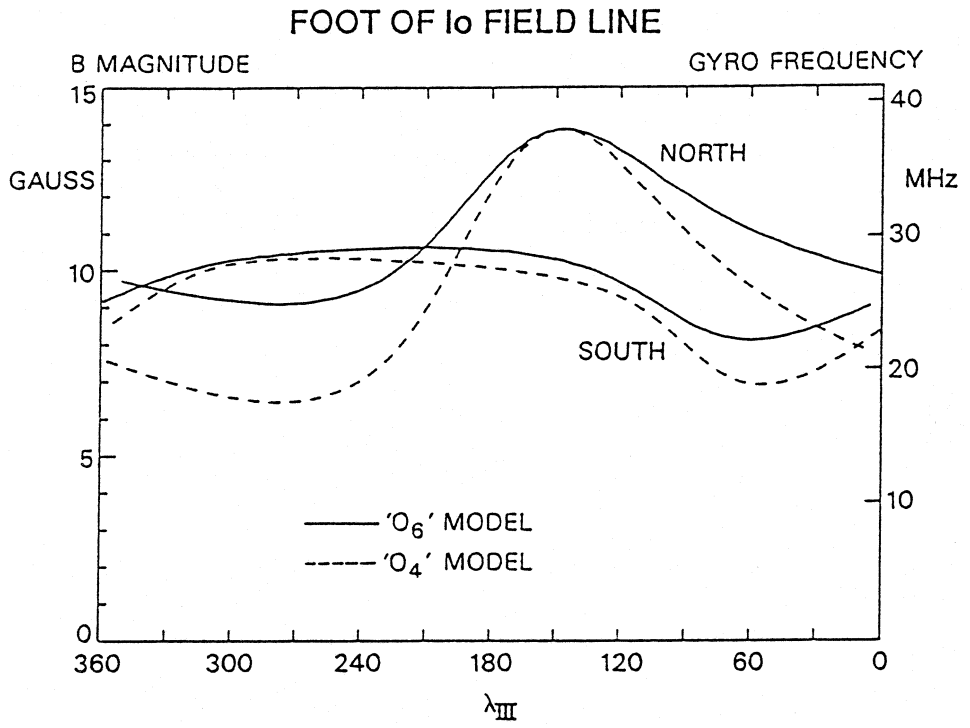

Figure 7: Surface magnetic field magnitude along the Io footprint (gyrofrequencies) as a function of longitude (λ_{III}), computed using the O_6 model (solid line) and the O_4 model of Jupiter's magnetic field.

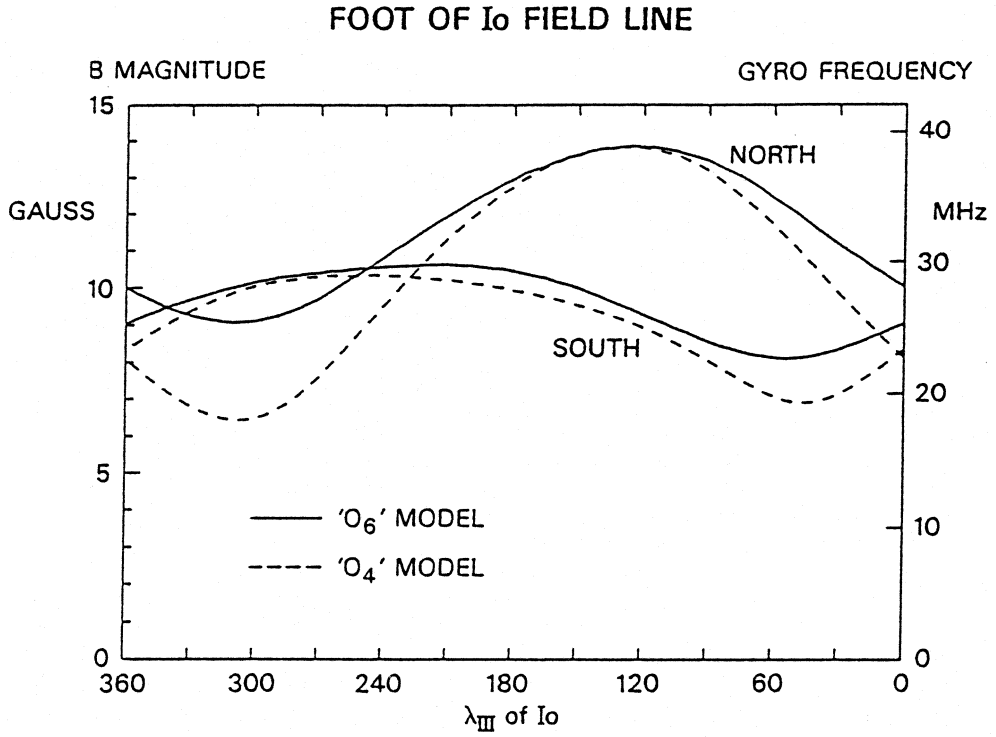

Figure 8: Surface magnetic field magnitude (gyrofrequencies) along the Io footprint as a function of Io's (λ_{III}) longitude (in the Jovigraphic equator), computed using the O_6 and O_4 models, as in Figure 7. This presentation differs from that of Figure 7 due to the 'bunching' of field lines towards regions of high field strength as they are mapped to the surface.

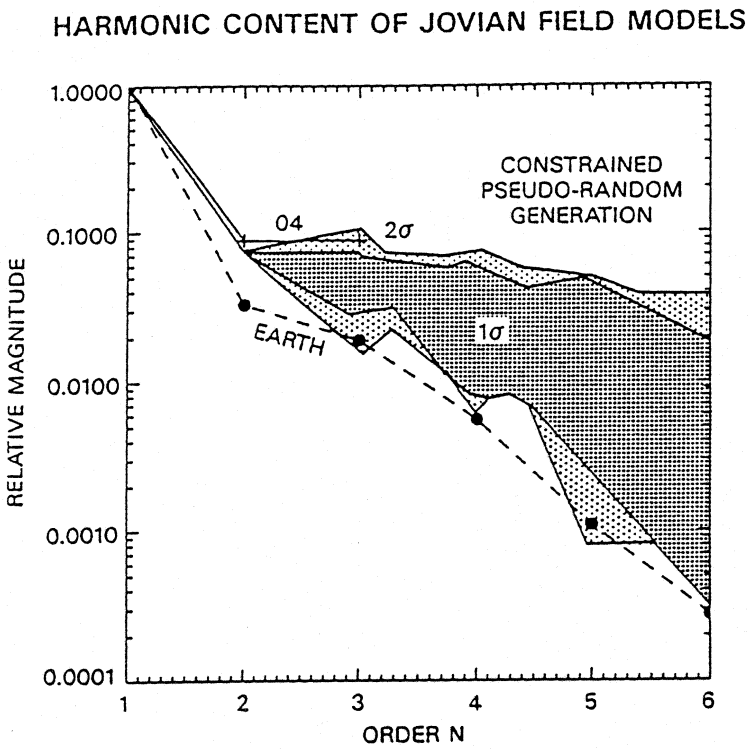

Figure 9: Normalized harmonic content of putative Jovian magnetic field models which are both 1.) consistent with in–situ P11 and V1 magnetic field observations at 1 or 2 standard deviations (1σ and 2σ) and 2.) characterized by harmonic spectra which decrease with increasing degree n for n>3.

We thus add an additional constraint: acceptable alternative models are required to have moments which decrease slightly with increasing degree. Any model generated by the above procedure that does not satisfy this additional constraint is rejected. The harmonic spectra of a suite of 100 alternative models which satisfy both the magnetic field observations and this new constraint fall within the shaded limits indicated in Figure 9 (1σ and 2σ respectively). These 100 models satisfy all we know, or think we know, about Jupiter's magnetic field; namely, they each provide acceptable fits to the in–situ observations, and they each have a 'reasonable' higher–order harmonic spectrum to n=6.

For each of the putative field models, we compute the location of Io's polar footprint, the magnitude of the field along the footprint, and the direction of the field along the footprint. This procedure should give us an estimate of the region of the polar surface accessible to the Io torus, as well as estimates of uncertainties in |B| and the direction of the field along

Figure 10: (next page, color plot) Orthographic (north) polar projection of the magnitude of the magnetic field on the surface of Jupiter computed using the O_6 model as in Figure 6. The region accessible to the foot of the Io field line is illustrated by tracing Io's field line foot for each of a hundred pseudo–randomly generated field models which are consistent (at 2σ) with the in–situ magnetometer observations of Pioneer 11 and Voyager 1 and subject to the constraint on higher–order multipoles illustrated in Figure 9. The poleward extent of the UVS slit at times of detection (closed circles) and non–detection (open circles) of the UV aurora is also indicated.

Figure 11: (following page, color plot) Orthographic (south) polar projection of the magnitude of the magnetic field on the surface of Jupiter, and the region accessible to the foot of the Io field line as in Figure 10.

the footprint. These estimates include 2σ errors (95% confidence) in the determination of model coefficients and uncertainties introduced by the presence of higher–order harmonics which are poorly constrained by available observations (but subject to the constraint on the moments). Figures 10 and 11 show north and south polar projections of these 100 Io footprints, superposed on a color background representing the surface field magnitude (O_6 model). The south polar region accessible to the Io torus spans a larger area and shows greater uncertainty in its location, compared to that in the north polar region, because the field magnitude in the south polar region is generally weaker than that in the north.

In order for the Io footprint region to be consistent with the inferred locations (being mindful of how these locations are inferred) of the UV aurorae, we require that the open circles (non–detection) lie equatorward of the poleward extent of the Io footprint. More precisely, the open points must either lie equatorward of the Io mapping region or within a standard error of observation (of the inferred source location of the UV auroral emissions). The latter is unknown, but the non–detection condition appears satisfied at all λ_{III}. We also require that all filled symbols (detection) lie poleward of the low–latitudinal extent of the Io mapping region. Again, filled points may lie equatorward of the Io mapping region if they lie within one standard error of observation (unknown). This condition appears to be satisfied at all λ_{III}, but for a few points at or near λ_{III}=0°. Whether these observations are also consistent with the hypothesis that the UV aurora occurs along the torus footprint depends on the error of observation of these few points. Figures 12 and 13 show orthographic projections of the aurorae and the Io mapping region from a vantage point in the Jovigraphic equator, much as observed by Voyager 2 during the UV mapping sequence. Figure 12 shows approximately how Jupiter appeared at 180° CML and Figure 13 shows how Jupiter appeared to an observer near the Jovigraphic equator at 0° CML. In Figure 13 we also have outlined, approximately, the footprint of the UVS observing slit, as appropriate for the Voyager 1 and Voyager 2 encounters; the difficulty in locating the source of polar auroral emission, particularly at 0° CML, is abundantly clear in this image. It appears that the UV auroral observations are fully consistent with a source location distributed along the Io footprint (or similar L).

Finally, Figure 14 illustrates the appearance of the planet, the Io mapping region, and the UV observations as the planet rotates through CML of 90°–180°.

Figure 12: (next page, color plot) Orthographic equatorial projection of the magnitude of the magnetic field on the surface of Jupiter computed using the O_6 model, as observed from the 'active' λ_{III} longitude of 180°. The region accessible to the Io foot (North and South) is shown as in Figures 10 and 11, as are the (inferred) positions of the UV aurora.

Figure 13: (following page, color plot) Orthographic equatorial projection of the Io footprint region, field magnitudes, and UV aurora on the surface of Jupiter as in Figure 12, but observed from the λ_{III} longitude of 0°. In this view the difficulties associated with locating observations near the planet's limb can be fully appreciated.

Figure 14: (following page, color plot) A montage of several orthographic equatorial projections of the Io footprint region, field magnitudes, and UV aurora as observed from CML of 90°, 120°, 150°, and 180°.

In Figures 15 and 16, we show the surface field magnitude and equivalent gyrofrequencies as a function of λ_{III} along the Io footprint for each of the putative field models in our suite. Field magnitudes at the foot of the field line are computed by tracing field lines from Io's position to the surface, for 20° increments of Io's λ_{III} (compares with Figure 7). The field lines, and therefore the computed values, are no longer equally–spaced in λ_{III} at the surface, but the clear vertical organization of the computed values indicates that the uncertainty in mapping Io's λ_{III} to the surface is $< 10°$ at most longitudes. Considerably higher surface field magnitudes (gyrofrequencies) may be encountered along the Io footprint, both north and south, compared to that computed using the O_6 model. The broad range of surface field magnitudes indicated here is possible only if the higher–order moments are as large as allowed by the constraint, but cannot be ruled out. Apparently, higher–order harmonics are relatively ineffective in shifting the position of the Io foot, but quite effective in altering the surface field magnitude along the foot. This is not unreasonable, if one considers that the influence of higher–order contributions is limited to the near surface region; local field properties are more easily altered by the higher–order harmonics than are global (mapping) properties. Finally, Figures 17 and 18 demonstrate that the local orientation of the field along the Io foot, compared to that of the O_6 model, may differ by some 10° to 20° in the northern and southern polar regions. In any event, the variation of these quantities along the foot may be expected to be dominated by the low order coefficients, similar to that obtained from the O_6 model in character, but shifted appreciably in magnitude and direction as a function of λ_{III}.

5 Summary

A base model for the magnetic field of Jupiter is obtained from Pioneer 11 and Voyager 1 observations using generalized inverse techniques applied to the estimation of planetary fields from spacecraft flyby observations. The model is obtained from a partial solution to the linear system of equations which relates spacecraft observations to model parameters. A sixth order spherical harmonic expansion is used to represent the internal (planetary) field; the field due to local (magnetodisc) currents is modeled using an empirical model representing a best fit to Voyager 1 observations. The dipole, quadrupole and octupole internal field coefficients are relatively well resolved, but higher–order parameters are little constrained by the combined Pioneer 11 and Voyager 1 magnetic field measurements.

Several quantities of interest in the study of Jupiter's magnetosphere are computed using a representative suite of putative Jovian field models. These are pseudo–randomly generated using the partial solution described above as a basic model, to which a random perturbation, which is both consistent with the in–situ magnetic field observations and constrained to have 'reasonable' higher–order moments, is added. For each model in the suite of models, we compute the position of the Io foot as a function of λ_{III}, as well as the magnitude and direction of the field as a function of position along the Io foot. In so doing we establish a polar region within which the foot of Io's field line must map, for any model which satisfies the magnetic field observations and a constraint on the magnitude of higher–order moments. A particular Io field line may be mapped to the polar region with an uncertainty of $\sim 10°$ or less. Similarly, we estimate reasonable uncertainties in

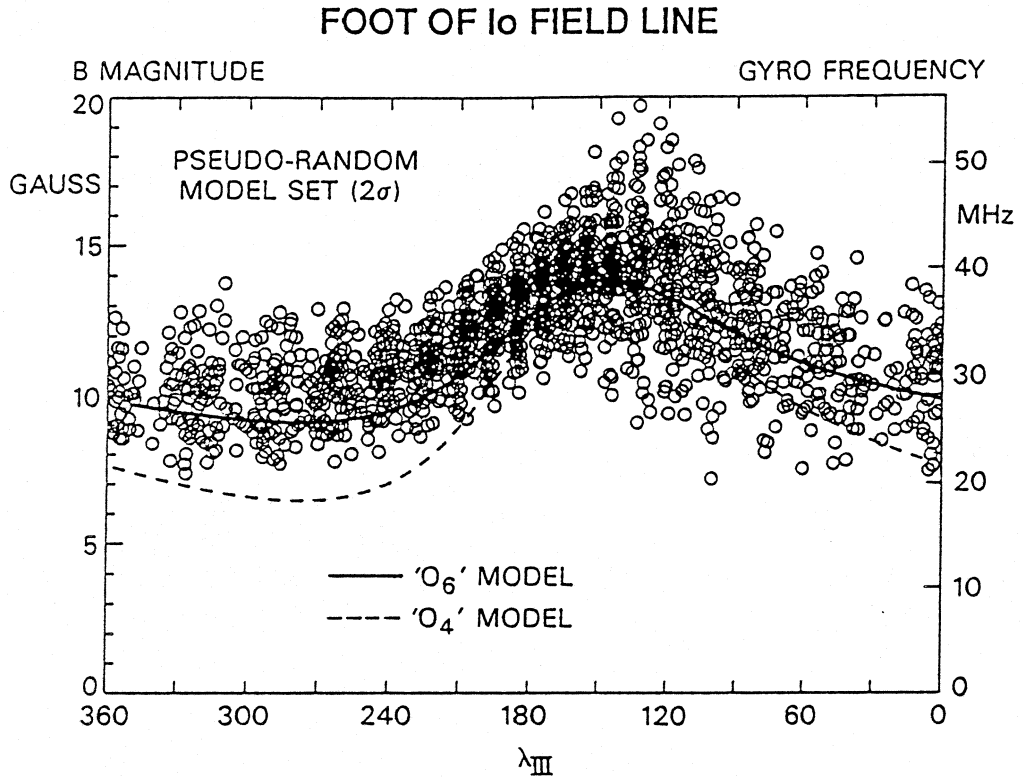

Figure 15: Magnitude of the magnetic field at the northern foot of Io's field line as a function of longitude (λ_{III}), computed using the suite of putative field models (open circles), compared with that computed using the O_6 (solid line) and O_4 (dashed line) models. The field line foot is computed for each 20° increment in Io's CML at Io's orbital position. The clear 'clumping' of such points as mapped to the surface indicates that Io's field line foot can be located with an error of less than about 10° along the track, depending on Io's λ_{III}.

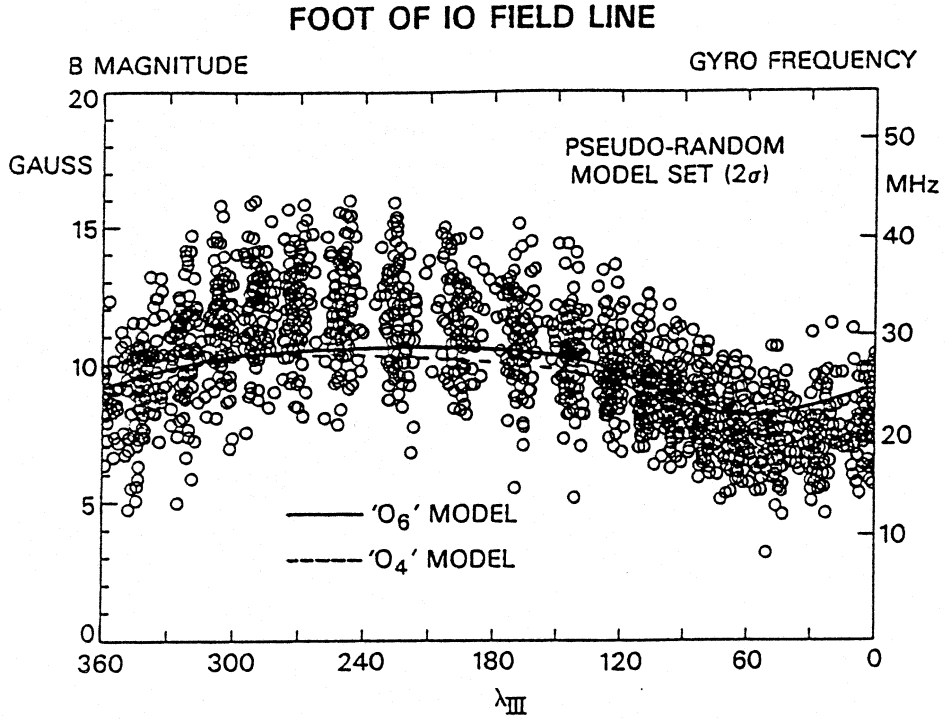

Figure 16: Magnitude of the magnetic field at the southern foot of Io's field line as in Figure 15.

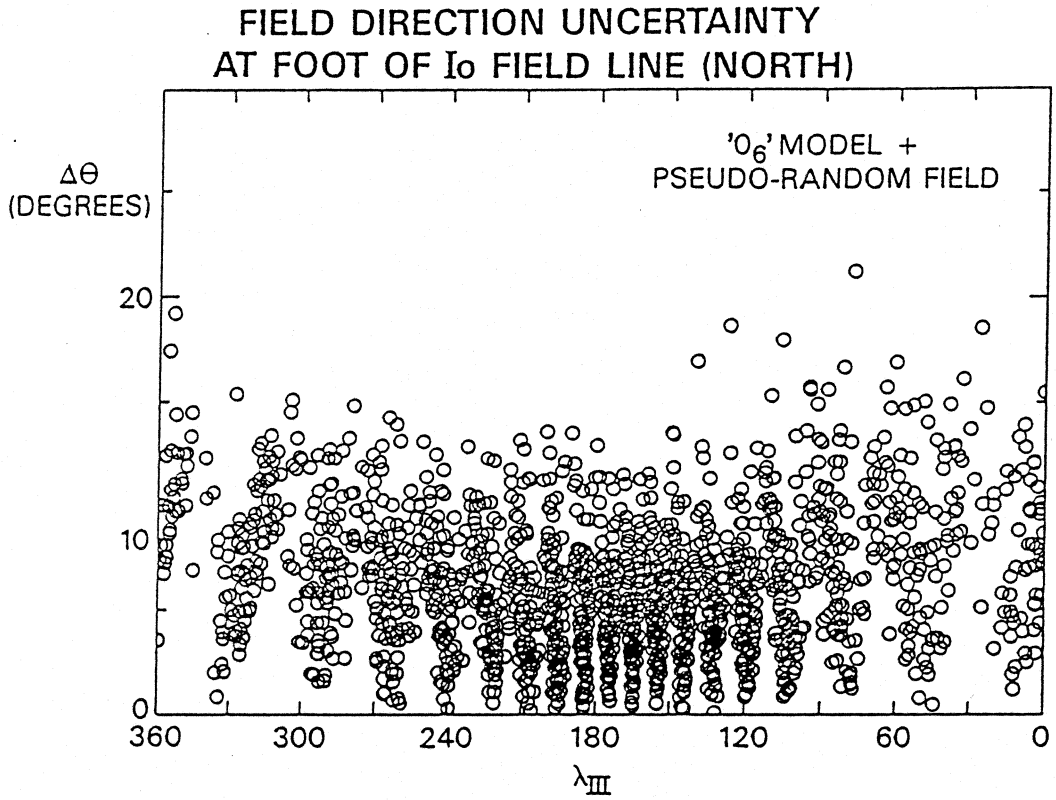

Figure 17: Angular difference (degrees) between the local field line direction along the northern Io foot as a function of longitude (λ_{III}), computed using the suite of putative field models (open circles), with respect to that computed using the O_6 model.

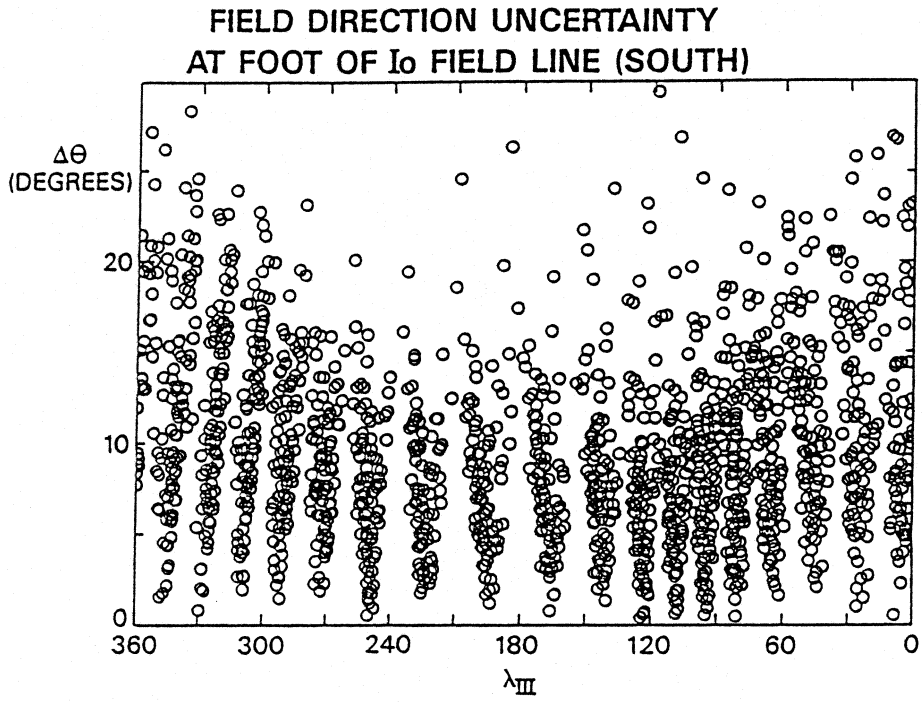

Figure 18: Angular difference (degrees) between the local field line direction along the southern Io foot as a function of longitude (λ_{III}), computed using the suite of putative field models (open circles), with respect to that computed using the O_6 model.

field magnitude and direction along the Io foot, subject to the same assumptions. In the North polar region, field magnitudes are likely (2σ) within ∼2 or 3 G of the nominal (O_6 model estimate) field magnitude; field directions are likely (2σ) within ∼10 to 20 degrees of the nominal field direction (O_6 model estimate).

The 'UV aurora', as located by Broadfoot et al. [1981], appears to be consistent with the North polar region accessible to the Io foot. Until a thorough analysis of the uncertainties associated with the inferred location of the UV aurora is available, it is not possible to address whether the UV observations may be used as an additional constraint on candidate Jovian field models. In contrast, a ∼70° shift in λ_{III} of gyrofrequencies at the foot of Io's field line, suggested by observations of Jovian DAM [e.g., Genova and Aubier, 1987; Genova and Calvert, 1988], appears highly unlikely for any reasonable Jovian field model. Subject to the constraints described above, it appears that there can be no more than ∼10° of uncertainty in λ_{III} in mapping along field lines from Io's orbital position to the North pole. An Io–initiated disturbance may be expected to propagate along an Alfvén wing, in the manner suggested by Gurnett and Goertz [1981], which will displace the disturbance towards lower λ_{III}, as required, by an amount that depends on the path length and density of the torus through which it propagates. Detailed calculations of the propagation of such a disturbance remain to be performed. However, it should also be emphasized that the peak frequencies displayed as a function of Io's λ_{III} (as in Figure 3) need not be simply related to the gyrofrequency at the foot of Io's flux tube; they are only the peak frequencies *visible* to an observer near the Jovigraphic equator for a particular alignment of Jupiter (in λ_{III}), Io (Io phase), and the observer. The observed events may in fact represent a distinct and rather peculiar minority of all emissions. It is reasonable to expect emissions at greater frequencies at practially any Io λ_{III} that are simply beamed away from the observer; Figures 15 and 16 would suggest that higher gyrofrequencies (> 40 MHz) are probably available along the Io foot.

References

Acuña, M. H., and N. F. Ness, Results from the GSFC fluxgate magnetometer on Pioneer 11, in *Jupiter*, ed. by T. Gehrels, University of Arizona Press (Tucson), 830–847, 1976a.

Acuña, M. H., and N. F. Ness, The main magnetic field of Jupiter, *J. Geophys. Res.*, **81**, 2917–2922, 1976b.

Acuña, M. H., K. W. Behannon, and J. E. P. Connerney, Jupiter's magnetic field and magnetosphere, in *Physics of the Jovian Magnetosphere*, ed. by A. Dessler, Cambridge University Press, Cambridge, Mass., 1–50, 1983.

Aubier, M. G., W. Calvert, and F. Genova, Source localization of Jupiter's Io–dependent Radio emissions, in *Planetary Radio Emissions II*, edited by H. O. Rucker, S. J. Bauer, and B. M. Pedersen, pp. 113–126, Austrian Academy of Sciences Press, Vienna, Austria, 1988.

Baron, R., R. D. Joseph, T. Owen, J. Tennyson, S. Miller, and G. Ballester, Imaging

Jupiter's aurorae from H3+ emissions in the 3–4 micron band, *Nature*, **353**, 539–542, 1991.

Birmingham, T. J., The Jovian magnetosphere, *Revs. Geophys. and Space Phys.*, **21**, 375–389, 1983.

Broadfoot, A. L., B. R. Sandel, D. E. Shemansky, J. C. McConnell, G. R. Smith, J. B. Holberg, S. K. Atreya, T, M. Donahue, D. F. Strobel, and J. L. Bertaux, Overview of the Voyager Ultraviolet Spectrometry results through Jupiter encounter, *J. Geophys. Res.*, **86**, 8259–8284, 1981.

Burke, L. F., and Franklin, K. L., Observations of a variable radio source associated with the planet Jupiter, *J. Geophys. Res.*, **60**, 213–217, 1955.

Caldwell, J., A. T. Yokunaga, and G. S. Orton, , Further observations of 8–micron polar brightenings of Jupiter, *Icarus*, **53**, 133–140, 1983.

Carr, T. D., M. D. Desch, and J. K. Alexander, The phenomenology of magnetospheric radio emissions, in *Physics of the Jovian Magnetosphere*, ed. A. J. Dessler, Cambridge Univ. Press, 226–284, 1983.

Caudal, G., and J. E. P. Connerney, Plasma pressure in the environment of Jupiter, infrared from Voyager 1 magnetometer observations, *J. Geophys. Res.*, **94**, 15055–15061, 1989.

Chapman, S. , and J. Bartels, *Geomagnetism*, pp. 639–668, Oxford University Press, New York, 1940.

Connerney, J. E. P., The magnetic field of Jupiter: A generalized inverse approach, *J. Geophys. Res.*, **86**, 7679–7693, 1981.

Connerney, J. E. P., The magnetospheres of Jupiter, Saturn, and Uranus, *Revs. Geophys. and Space Phys.*, **25**, No.3, 615–638, 1987.

Connerney, J. E. P., M. H. Acuña, and N. F. Ness, Modeling the Jovian current sheet and inner magnetosphere, *J. Geophys. Res.*, **86**, 8370–8384, 1981.

Connerney, J. E. P., and M. H. Acuña, Jovimagnetic secular variation, *Nature*, **297**, 313–315, 1982.

Connerney, J. E. P., M. H. Acuña, and N. F. Ness, Voyager 1 assessment of Jupiter's planetary magnetic field, *J. Geophys. Res.*, **86**, 3623–3627, 1982.

Connerney, J. E. P., M. H. Acuña, and N. F. Ness, The magnetic field of Neptune, *J. Geophys. Res.*, **96**, 19023–19042, 1991.

Davis, L. jr., D. E. Jones, and E. Smith, The magnetic field of Jupiter, Presented at AGU fall meeting, San Francisco, 1975 (see review by Acuña et al., 1983).

de Pater, I., Observations and models of the decimetric radio emission from Jupiter, *Ph. D. thesis*, State University of Leiden, Leiden, 1980.

de Pater, I., and W. J. Jaffe, Very large array observations of Jupiter's non–thermal radiation, *Astrophys. J. Suppl.*, **54**, 405–419, 1984.

Genova, F. and M. G. Aubier, High frequency limit and visibility of the non–Io and Io–dependent Jovian decameter radio emission, *Astron. Astrophys.*, **177**, 303–309, 1987.

Genova, F., and W. Calvert, The source location of Jovian millisecond radio bursts with respect to Jupiter's magnetic field, *J. Geophys. Res.*, **93**, 979–986, 1988.

Gurnett, D. A., and C. K. Goertz, Multiple Alfvén wave reflections excited by Io: Origin of the Jovian decametric arcs, *J. Geophys. Res.*, **86**, 717–722, 1981.

Kim, S. J., P. Drossart, J. Caldwell, J.-P. Maillard, T. Herbst, and M. Shure., Images of aurorae on Jupiter from H3+ emissions at 4 microns, *Nature*, **353**, 536–539, 1991.

Langel, R. A., The main field, in *Geomagnetism*, **Vol. 1**, ed. J. A. Jacobs, Academic Press (London), 249–513, 1987.

Langel, R. A., and R. H. Estes, A geomagnetic field spectrum, *Geophys. Res. Lett.*, **9**, 250–253, 1982.

Lowes, F. J., Spatial power spectrum of the main geomagnetic field and extrapolation to the core, *Geophys. J. R. Astron. Soc.*, **36**, 717–730, 1974.

McNutt, R. L., jr.,The magnetospheres of the outer planets, *Rev. geophys.*, supplement, 985–987, 1991; U.S. National Report to IUGG 1987-1990.

Schneider, N. M., J. T. Trauger, J. K. Wilson, D. I. Brown, R. W. Evans, and D. E. Shemansky, Molecular origin of Jupiter's fast Sodium, *Science*, **253**, 1394–1397, 1991.

Smith, B. A., L. A. Soderblom, T. U. Johnson, A. P. Ingersoll, S. A. Collins, E. M. Shoemaker, G. E. Hunt, H. Masursky, M. H. Carr, M. E. Davies, A. F. Cook (II), J. Boyce, G. E. Danielson, T. Owen, C. Sagan, R. F. Beebe, J. Veverka, R. G. Strom, J. F. McCauley, D. Morrison, G. A. Briggs, V. E. Suomi, The Jupiter system through the eyes of Voyager 1, *Science*, **204**, 948–972, 1979.